THE PENNSYLVANIA STATE UNIVERSITY
SCHREYER HONORS COLLEGE

DEPARTMENT OF GEOSCIENCES

# IMPURITY INFLUENCE ON NORMAL GRAIN GROWTH AND CONDUCTANCE IN THE WAIS DIVIDE 06A ICE CORE, ANTARCTICA

NATHAN T. STEVENS
SPRING 2013

A thesis
submitted in partial fulfillment
of the requirements
for a baccalaureate degree
in Geosciences
with honors in Geosciences

Reviewed and approved* by the following:

Richard B. Alley
Evan Pugh Professor of Geosciences
Thesis Supervisor

Peter J. Heaney
Professor of Geosciences
Honors Adviser

* Signatures are on file in the Schreyer Honors College.

# ABSTRACT

High impurity loading leads to reduced grain-growth rates in the WAIS Divide 06A ice core, West Antarctica, as shown by regression analysis of new data from this core. Grain-sizes measured on thin sections cut from the core were compared to concentrations of soluble and insoluble impurities measured on the remaining core over the same depth intervals. Comparisons were also made with the electrical conductivity of the ice (ECM). In general, samples with higher concentrations of several impurities, especially calcium, but also magnesium, sodium, and sulfate, showed smaller grain-sizes. Physical understanding indicates that higher impurity loading reduces the grain-growth rates. While some impurities increase electrical conductivity, others decrease it, which resulted in a noisy dependence of ECM on impurity loading observed in this work.

# TABLE OF CONTENTS

# LIST OF FIGURES

# LIST OF TABLES

# ACKNOWLEDGEMENTS

I thank J. Fitzpatrick, J. Fegyvereis, I. Chong, and D. Laurel for their preparation and analysis of samples, J. McConnell, J. Cole-Dai, and co-workers for unpublished chemical data, and K. Taylor and co-workers for unpublished electrical conductivity data. I also thank the WAIS Divide Science Coordination Office, the National Ice Core Lab (NICL), and assorted WAIS Divide colleagues for their assistance and logistical support, and the National Science Foundation Polar Programs for financial support under grant 1043528. Additionally, I thank Dr. Richard Alley and Dr. Rita Stevens for their critical insights and commentary.

# Chapter 1

# Introduction

Ice flow modeling is a critical tool for interpreting past, and forecasting future, atmospheric and cryospheric dynamics. Models are particularly important to ice-core based paleoclimate studies, as they provide important information for depth-age models to which paleoclimate data are referenced. These models' flow laws are derived, in part, from observations of glacier ice's physical properties (Alley 1992, Alley et al. 1995). The grain-area[1] of ice and grain-growth trends are of particular interest as they dictate the behavior of other physical properties, and they are used to interpret the microscopic deformation processes that facilitate glacier flow (Alley 1992).

As discussed by Alley et al. (1986a), normal grain growth in glacier ice is interpreted, in part, using grain-area populations measured from a series of optical thin sections from ice cores. Simple physical relations, originally developed in metallurgy, suggest that grain-area should increase approximately linearly with time; this is often called "normal grain growth" (Gow 1969, Alley et al. 1986a). Deviations from normal growth trends are controlled by variation of several parameters including: temperature and temperature variations, differential stresses (particularly basal shear), and impurity concentrations (Alley 1992 and references therein). While experiments on laboratory ice reveal much about the influence of these variables on grain growth, those experiments cannot emulate the sample age-range encompassed by glacier ice: $10^0$ to $10^5$ years (Alley et al. 1986a). It is for this reason that studies of glacier ice are imperative to further constrain the suite of flow laws used in glacier flow models. Studies by Alley et al. (1986a,b),

[1] The term "grain" is analogus to crystal in this work. This convention comes from the metallurgical literature (Gow 1969 and Alley et al. 1986a).

Alley et al. (1995), Alley & Woods (1996), and Durand et al. (2006) examined controls on normal grain growth at sites where temperatures and stresses are well characterized. These characterizations permitted investigation of the influence of various levels of impurity loading, including both soluble (aqueous ions) and insoluble (dust and intergranular bubbles) impurities with minimal influence on grain-areas from these other parameters.

This work extends these studies by investigating the influence of soluble impurities on grain-growth trends for a ~2.1 km span of the West Antarctic Ice Sheet (WAIS) Divide 06A Ice Core (WDC 06A) using grain-area and ion-concentration data from ongoing studies of the core (Fitzpatrick pers-comm, Cole-Dai 2012, McConnell pers-comm). The WAIS Divide core was drilled as part of a National Science Foundation-sponsored project to collect a deep ice core to near bedrock in a high-accumulation site, providing a record equivalent to those collected from central Greenland, including GISP2, in terms of accumulation rate, deformation, and temperature history. As such, this work sought to further the studies of Woods (1994) and Alley & Woods (1996) on GISP2 by using newly available datasets from the WDC 06A core to characterize correlations between soluble impurity loading and grain-growth trends.

Earlier studies (particularly Alley & Woods, 1996 and references therein) found a “noisy yet statistically significant” inverse relationship between grain-size and impurity loading in ice cores, suggesting that impurities inhibit grain-boundary migration (Alley et al. 1986a). This work compares chemical and grain-size data utilizing the ice-core chemistry measured in two separate labs, each with different spatial resolutions and analyzed chemical species, as described in the methods section (Chapter 2, Part I, Section C). Additionally, impurities exert a large influence on electrical conductivity measurements (ECM) in ice cores (Taylor et al. 1993, Sugiyama et al. 2000, and Barnes & Wolff 2004). Those studies recorded decreased conductivities in alkaline ice, associated with terrestrial dust content (Taylor et al. 1993), and increased conductivity in acidic ice, associated with volcanic layers (Sugiyama et al. 2000 and Barnes & Wolff 2004). This

current work expands on those earlier studies by integrating ECM data from the WDC 06A core (Taylor et al. 2011) with grain-size and impurity concentration data.

In summary, this work sought to characterize relationships among grain-area, soluble impurity loading, and conductivity data for the WDC 06A ice core. These relationships have been characterized for similar ice cores in central Greenland (particularly GISP2) by several independent studies, which played a role in establishing climate records and deriving ice flow laws for cryosphere modeling. Statistically significant correlations between grain-size and impurity loading in for the WDC 06A ice core might serve to better constrain the contribution of impurity loading to deviations from normal grain-growth when interpreting microscopic deformation processes at play (Alley 1992). Similar correlations between ECM and impurity loading or grain-area would further improve the interpretation of ice core records, refining the observations of Taylor et al. (1993), and providing new insights to the relationship between the physical and electrical properties of glacier ice. Such relationships, should they be significant, might be applied to identify sections of ice core for further study or even serve as a proxy for grain-area. The absence of statistically significant relationships would also contribute to our understanding of glacier ice.

# Chapter 2

# Methods

## I) Site Location & Dataset Descriptions

### *A) WAIS Divide Site and Ice Core*

The WAIS Divide drilling site is located at 79° 28.058' S, 112° 05.189' W, at ~1806m above sea level, 24km down slope from the West Antarctic flow divide (shown as a dashed line near WAIS Divide in **Figure 2-1**). Further site information is available at http://waisdivide.unh.edu. Samples used in this work were collected from the WDC 06A ice core, which were drilled during the Antarctic summers of 2007/08 – 2011/12 to a depth of 3406m below the surface datum. This work makes use of data from 579m to 2686m because complete data were not available for other depths.

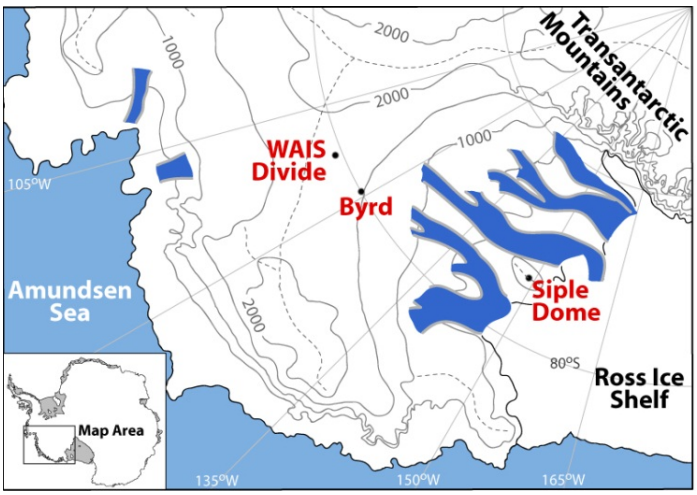


**Figure 2-1: WAIS Divide Site Location (from Conway)**

### *B) Grain-Area Populations*

This work employed grain-area populations from 86 vertical thin sections (VTS) analyzed by Fitzpatrick et al. (pers-comm). VTS consist of ~10cm depth spans sampled every

~20m within WDC 06A. All thin sections were prepared, photographed in cross-polarized light, and analyzed using image-processing software to digitalize grain boundary geometries per Fitzpatrick's methods (2013) at the National Ice Core Laboratory (NICL) by Fitzpatrick et al. (pers-comm). There were between 450 and 1998 grains per VTS with an average of 892 grains, providing a large enough sample to constrain grain-size with high confidence and little uncertainty (Fitzpatrick & Alley 2012). Grains were characterized using x-centroid and area statistics reported in the data by Fitzpatrick et al. (pers-comm). The centroid represents the arithmetic mean of all points within a given measured grain, and area represents the size of the grain. The x-centroid was selected to represent the depth of a given grain as VTS were analyzed with the left side of the slide as stratigraphic up (Fitzpatrick 2013). This permitted an adaptation of the horizontal intercept method of analysis used by Alley & Woods (1996) to determine mean grain-size for a given depth interval in the ice core.

***C) Soluble Impurity Concentrations***

The depth range of WDC 06A analyzed in this work encompasses two impurity datasets from the WAIS Divide project. The first dataset reported major ion chemistry of the core between 577m and 1300m in μg/kg every 2-3cm (Cole-Dai 2012). Chemical species analyzed in that study included sodium (Na), magnesium (Mg), chloride (Cl), nitrate ($NO_3$), sulfate ($SO_4$), and non-sea-salt sulfate (reported as nss$SO_4$, but discussed here as nssS). These species include impurities sourced from sea salt, aerosols, and some terrestrial input (as discussed in Chapter 4) captured during snowfall and snow densification (Cuffey & Paterson 2010). The second dataset analyzed trace and ultra-trace chemistry for the remainder of the core (McConnell pers-comm). McConnell specifically provided concentration values for Na, non-sea-salt sulfate (nssS), non-sea-salt calcium (nssCa), cerium (Ce), and black carbon (BC) for this work. These species serve as

metrics for several soluble impurity inputs including sea salt (Na), aerosol (nssS), terrestrial dust (nssCa & Ce), and biomass burning (BC) (Cuffey & Paterson 2010, Alley pers-comm). These data were reported in parts per billion (PPB) every 2cm, resulting in 5 values per VTS.

To distinguish between these two datasets, analyses between 579m-1300m are dubbed "Shallow" while those between 1300m-2700m are dubbed "Deep". While these datasets do not permit correlation of all species across the ~2.1km span addressed in this work, metrics for sea salt input (Na) and aerosol input (nssS) were available for analysis for the entire core. Additionally, Shallow data were converted to PPB to match the units of the Deep data. Impurity species used in this work and their associated datasets are summarized in Table 2-1**.**

**Table 2-1: Soluble Impurity Speciation Symbols and Distribution**

| Symbol | Impurity Name | Shallow | Deep |
|---|---|---|---|
| [Na] | Sodium Ion | X | X |
| [nssS] | Non-Sea-Salt Sulfate Ion | X | X |
| [$SO_4$] | Sulfate Ion | X | |
| [$NO_3$] | Nitrate Ion | X | |
| [Cl] | Chloride Ion | X | |
| [Mg] | Magnesium Ion | X | |
| [nssCa] | Non-Sea-Salt Calcium Ion | | X |
| [Ce] | Cerium Ion | | X |
| [BC] | Black Carbon | | X |

***D) Electrical Conductivity Measurements***

This work employed ECM reported by Taylor (2011) between 550m and 2700m at a frequency of ~1mm; this resulted in ~100 values per VTS. Due to changes in electrode design between analysis seasons (Taylor pers-comm), these data form two distinct depth subgroups: 550m-1350m and 1350m-2700m. These data further constrained the Deep dataset to the depth range of 1360m-2683m for correlation purposes.

## II) Data Preparation

### *A) Data Import and Depth Correlation*

All datasets were initially formatted as Microsoft Excel (.xlsx) with the exception of conductivity data, which were formatted as text files and then converted to .xlsx format using Excel's import menu. All data were then imported into MATLAB using the *xlsread.m* function. Impurity concentration and conductivity values were sub-sampled to include only those data that lay within the depth ranges covered by grain-area data (see Appendix A, Table 6-7).

While importing grain-area data into MATLAB, the x-centroid ( $XCentroid_i$ ) value of each grain was converted to an absolute depth ( $Feature\_Depth_i$ ) using equation 1 (units shown in brackets),

$$(1) \qquad Feature\_Depth_i[m] = \frac{XCentroid_i[cm] - XCentroid_{min}[cm]}{100\ [\frac{cm}{m}]} + VTS_{Depth}[m]$$

where $XCentroid_{min}$ represents the lowest x-centroid value in a given VTS and *VTS_Depth* represents the shallowest depth included in the VTS (tabulated in Appendix A, Table 6-7 as "Top Depth").

Deep soluble impurity data included a standard reported value of -0.999 for concentrations where a given species was not recorded, as opposed to the value of 0 for observations of zero concentration. These "not-recorded" values constituted less than 10% of all data sampled and were converted to NaN in MATLAB to maintain the data structure while removing the values from calculations of means, standard deviations, and linear regressions. There was one reported negative value in the Shallow impurity concentration dataset (Cole-Dai 2012), which was manually also converted to a NaN value.

Due to several gaps in reported values (on the scale of 4-10cm) dispersed through the datasets used in this work, several VTS within the 579m-2686m depth range were omitted due to insufficient data to produce viable correlations. These omissions are represented by deviations from the standard ~20m sampling frequency in the sample log (Appendix A, Table 6-7). This data limitation further constrains the Shallow dataset to the depth range 579m-1245m and the Deep dataset to the depth range 1362m-2683m.

***B) Data Resampling***

This work employed linear regressions to characterize the statistical significance and nature of relationships between grain-size, impurity loading, and ECM. This was accomplished using the *LinearModel.fit* function in MATLAB, which required all input datasets to have the same spatial resolution. Upon intake, spatial resolution varied by 1-2 orders of magnitude between datasets (Grain-Size > ECM > Impurity Concentration), which required resampling of grain-size data (spatial resolution of $10^2$ to $10^3$ samples per VTS) and ECM data (spatial resolution of $10^1$ to $10^2$ samples per VTS) to match the spatial resolution of impurity concentration data ($10^0$ to $10^1$ samples per VTS). Resampling was conducted by taking the mean value of grain-size and ECM values that fell within at ±0.5cm depth window centered on the reported depth of each impurity concentration value.

The ±0.5cm depth window was selected for resampling grain-areas because it averages ~90 grains per point, which is sufficient to determine average grain-area ($\bar{A}$) to within a few percent (Alley & Woods 1996). This approach was intended as a modification of the horizontal intercept method for determining $\bar{A}$ used in several studies (e.g. Gow 1969, Alley et al. 1986a,b, Alley & Woods 1996). This value was also applied to ECM data as it accounts for the ~1cm current dispersion that occurs when sampling conductivity across an ice core (Alley, pers-comm).

***C) Analytic Frames***

This work partitioned data according to 7 "analytic frames" for statistical analysis at 4 separate spatial resolutions[2]. These frames include Full Core Mean Vertical Thin Section sampling (FC-MVTS), Shallow and Deep Mean Vertical Thin Section sampling (S-MVTS and D-MVTS), Shallow and Deep Vertical Thin Section sampled in 100m bins (S-VTS100 and D-VTS100), and Shallow and Deep Vertical Thin Section data sampled for every VTS (S-VTS and D-VTS). The FC-MVTS analytic frame includes grain-area, [Na], and [nssS] data for the entire core, resulting in 86 data points spanning the entire core. The S-MVTS and D-MVTS analytic frames include the mean value for all data (grain-area, ECM, and all impurity species) within each VTS (assigned the mean depth value of the section), resulting in 25 data points in the Shallow depth range (579m-1245m) and 61 data points in the Deep depth range (1362m-2683m). These analytic frames address large spatial trends between datasets in the WDC 06A core, but they are also subject to variations in temperature and deformation history characterized throughout the core that affect grain-gowth trends (Alley pers-comm).

The S-VTS100 and D-VTS100 analytic frames grouped data into 100m depth bins, producing 7 bins for Shallow data and 14 bins for Deep data with an average of 25 data points for each dataset per bin. This analytic frame constrains the spatial sampling for each model enough to greatly reduce the possible influence of controls on grain-area other than impurity loading (Alley pers-comm). These bins and their contents are tabulated in Table 6-7 (Appendix A). The S-VTS and D-VTS analytic frames assessed each VTS as a sampling bin, producing 25 bins for Shallow data and 61 bins for Deep data, each consisting of 3-5 data points for all data. While these analytic frames have sparse data, the 10cm sampling range for each model effectively eliminates

[2] This is not to be confused with the spatial-resolution discussed for data resampling (Chapter 2, Part I, Section A) as all data types used in these analytic frames have the same spatial resolution imparted to them by resampling.

all other influences on grain-area within a given sample except impurity loading (Alley pers-comm).

## III) Statistical Modeling and Analysis

### *A) Linear Regression Modeling*

All dataset elements were paired for linear regression as tabulated in Table 2-2. Linear regressions were conducted in each analytic frame for each "data pair" using "RobustOpts" operator in *LinearModel.fit* to reduce the statistical weighting of outliers. Linear regressions were conducted for every data pair in each bin for analyses in the S-VTS100 and D-VTS100 analytic frames and for every data pair in each VTS for analyses in the S-VTS and D-VTS analytic frames. The series of models produced in these analytic frames formed "model sets" for each data pair.

**Table 2-2: Linear Regression Data Pair Naming Scheme**

| | | Parameter 1 | |
|---|---|---|---|
| Parameter 2 | --- | Grain-Area | ECM |
| | **Sodium** | Ā/[Na] | ECM/[Na] |
| | **nss Sulfate** | Ā/[nssS] | ECM/[nssS] |
| | **Sulfate** | Ā/[SO4] | ECM/[SO4] |
| | **Nitrate** | Ā/[NO3] | ECM/[NO3] |
| | **Chloride** | Ā/[Cl] | EMC/[Cl] |
| | **Magnesium** | Ā/[Mg] | ECM/[Mg] |
| | **nss Calcium** | Ā/[nssCa] | ECM/[nssCa] |
| | **Cereum** | Ā/[Ce] | ECM/[Ce] |
| | **Black Carbon** | Ā/[BC] | ECM/[BC] |
| | **ECM** | Ā/ECM | --- |

***B) Model Characterization***

This work described relationships between data pairs using their models' slope and p-value statistics. The sign of a model's slope, called polarity in this work, characterized its data pair's trend as either positive (direct relationship) or negative (inverse relationship) while the model's p-value described the trend's statistical significance. MATLAB employs a p-value notation where low values represent high statistical certainty (i.e. a p-value = 0 means 100% certainty that the linear regression is fit to an actual trend in the data, while a p-value = 1 means a line fit to random data, 0% certainty). Using this convention, the trends of each data pair were assessed for statistical significance based upon their p-values.

***C) P-Value Filtering***

This work employed "p-value filters" to differentiate the statistical significance of data pairs. This system of differentiation is referred to as "scaled statistical significance" (SSS) in this work, which consists of "high", "moderate", "low", and "very low" statistical-significance ratings. Models with p-values less than 0.1 were deemed to have "high significance trends", models with p-values less than 0.3 were deemed "moderate significance trends", and those models with p-values greater than 0.3 were deemed to have "low significance trends". In the case of very high p-values (0.85 and greater), models were deemed to have "very low significance trends". These values were selected in order to represent 70% (p-values $\leq 0.3$) and 90% (p-values $\leq 0.1$) confidence intervals for statistical significance, and as a way to differentiate weak correlations from even weaker correlations (low significance vs. very low to zero significance).

***D) Model Set Characterization***

While data relationships in the FC-MCTS, S-MVTS, and D-MVTS analytic frames were described according to the p-value and slope polarity for a single model of each data pair, relationships in analytic frames that produced model sets (S-VTS100, D-VTS100, S-VTS, and D-VTS) were assessed in terms of their "polarity sum" and "sample-ratio". These metrics communicate the distribution of polarities in a set of models as a function of the p-value filters described above. After applying a given p-value filter, the those models with sufficient significance were used to describe a data pair's net polarity by taking the sum of positive (assigned value of +1) and negative (assigned value of -1) trends. The polarity sum's sign characterizes the data pair's dominant polarity (positive or negative) while the magnitude of the sum describes consistency of reported trend across sampling bins in an analytic frame. For example: a p-value filtered model set with a large, positive polarity sum would consist of many positive trends and few or no negative trends, thereby communicating that the data's relationship is dominantly modeled as positive in a given analytic frame.

The "sample-ratio" (SR) states the ratio of the number of models after applying a p-value filter to the total number of models in a set. This communicates the overall statistical significance of the model. That is to say, a model set with a high sample-ratio after applying a p-value filter would be considered a set with an overall SSS rating associated with the filter applied. While the analytic frames that are described using sample ratio and polarity sum were assigned the same significance designations as the MVTS frames, these metrics act as simplified assessment of data pair's relationship (having little quantitative bearing). However, they do serve to identify and qualitatively characterize those data pairs with statistically significant correlations for additional analysis.

# Chapter 3

# Results

## I) Linear Regression Modeling Results

### *A) Full Core Mean VTS Correlation Results*

Linear regressions produced from Ā, [Na], and [nssS] sampled in the FC-MVTS analytical frame are shown in Figure 3-1. The model of Ā/[Na] estimated the relationship as [ - 407.94 x + 47.003 ] with a slope p-value of $2.1390*10^{-7}$. The model of Ā/[nssS] estimated the relationship as [ -88.9x + 21.74 ] with a slope p-value of 0.12674.

**Figure 3-1: FC-MVTS Linear Models for Ā/[nssS] and Ā/[Na]**

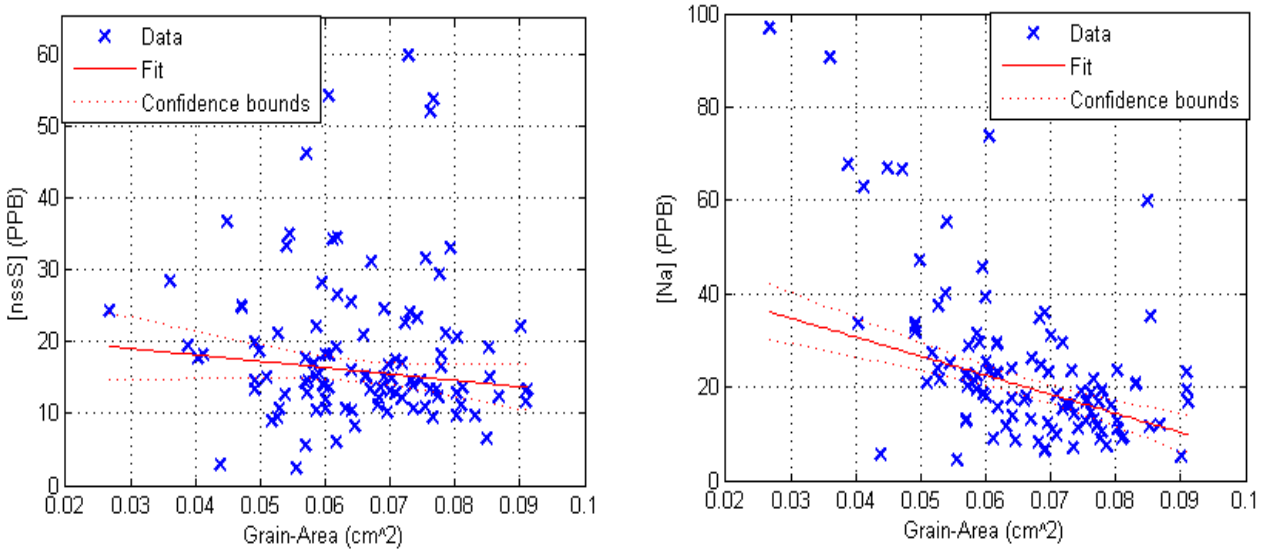

***B) MVTS Linear Regression Statistics***

Statistics from models in the S-MVTS and D-MVTS analytical frames are presented in Table 6-1 and Table 6-2, respectively (Chapter 6, Appendix A). These tables report the slope and p-value from models of each data pair and additionally report the mean value and 1 standard deviation for each parameter that composes a given data pair. The high significance trends in the S-MVTS analytic frame included the models: ECM/[$SO_4$], ECM/[nssS], ECM/[$NO_3$], which had positive polarities, and the models $\bar{A}$/[Na], $\bar{A}$/[Mg], $\bar{A}$/[$SO_4$], and $\bar{A}$/[Cl], which had negative polarities. The high significance trends in the D-MVTS analytic frame included the models: ECM/[nssS], which had a positive polarity, and $\bar{A}$/[Na], $\bar{A}$/[nssS], $\bar{A}$/[Ce], and $\bar{A}$/[nssCa], which had negative polarities. In the S-MVTS and D-MVTS analytic frames, the models for $\bar{A}$/ECM had a positive polarity very close to moderate significance (p-value = 0.3109) in the S-MVTS analytical frame and positive, moderate significance relationship (p-value = 0.2864) in the D-MVTS analytic frame. The scaled statistical significance of all models in these analytic frames are tabulated in Table 3-1.

***C) VTS100 Linear Regression Statistics***

Statistics from linear regressions in the S-VTS100 and D-VTS100 analytical frames are presented in Table 6-3 and Table 6-4, respectively (Chapter 6, Appendix A). These tables present trend count (positive and negative), trend sum, and sample ratio statistics before filtering and after applying filters for p-values less than 0.3 and p-values less than 0.1. The high significance model sets in the S-VTS100 analytic frame included ECM/[$NO_3$], ECM/[nssS], and ECM/[$SO_4$], which had positive polarities with high sample ratios when filtered, and models for $\bar{A}$/[Mg], $\bar{A}$/[Na], and $\bar{A}$/[Cl], which small negative polarity sums when filtered. The small polarity sums of these model

sets indicate variability in polarity amongst their models' trends. The most significant model sets in the D-VTS100 analytic frame included ECM/[nssS] and ECM/[Na], which had large positive polarity sums. Similarly, Ā/[nssS], Ā/[Ce], and Ā/[nssCa] had large, negative polarity sums with high sample ratios when filtered.

Models for Ā/ECM in S-VTS100 produced a small, negative polarity sum with a low sample ratio when filtered for moderate significance (p-values $\leq 0.3$). Models in D-VTS100 produced a small positive polarity sum when filtered for moderate and high significance. These suggest statistically weak correlations with variable polarity. The remaining data pairings produced model sets where the sample ratio approached 0 after the p-value $\leq 0.3$ filter or reported sums that had low magnitude and variable polarities when filtered. The scaled statistical significance of all models in these analytic frames are tabulated in Table 3-1.

***D) VTS Linear Regression Statistics***

Statistical data from models in the S-VTS and D-VTS analytical frames follows the same structure and conventions as those for the VTS100 analytical frames. These data are presented in Table 6-5 and Table 6-6 for S-VTS and D-VTS respectively (Chapter 6, Appendix A). The most significant trends in the S-VTS analytic frame were ECM/[$NO_3$], ECM/[$SO_4$], and ECM/[nssS], which had large positive net polarities. Similarly, Ā/[Mg], Ā/[$SO_4$], and Ā/[nssS] had large negative polarity sums in this analytical frame. The high significance relationships in the D-VTS analytic frame were ECM/[nssS], ECM/[Na], and ECM/[Ce], which had large positive polarity sums. Contrary to other analytical frames' data, Ā/[nssS] and Ā/[nssCa] also had positive polarity sums with magnitudes 2 and 4 respectively when filtered for high SSS (p-values $\leq 0.1$). The model for Ā/ECM in S-VTS had a zero polarity sum at both the 0.1 and 0.3 significance filters. Additionally, models for Ā/ECM in the D-VTS analytic frame had large, positive polarity sums

when filtered at high significance. The scaled statistical significance of all models in these analytic frames are tabulated in Table 3-1.

## II) Results Summary

The scaled statistical significance (SSS) rating of each data pairing for all analytic frames are tabulated in Table 3-1. The signs, (+) and (-), are included in this table to represent the polarity, or most significant non-zero polarity sum, for each model.

**Table 3-1: Summarized Linear Model Relative Relevance: All Analytic Frames**

| **Analytic Frame** | | | | | | |
|---|---|---|---|---|---|---|
| ***FC-MVTS*** | ***S-MVTS*** | ***D-MVTS*** | ***S-VTS100*** | ***D-VTS100*** | ***S-VTS*** | ***D-VTS*** |
| Ā/[Na] (-) | ECM/[$NO_3$] (+) | Ā/[Na] (-) | ECM/[$NO_3$] (+) | ECM/[nssS] (+) | ECM/[$NO_3$] (+) | ECM/[nssS] (+) |
| Ā/[nssS] (-) | Ā/[Na] (-) | Ā/[nssS] (-) | ECM/[nssS] (+) | ECM/[Na] (+) | ECM/[$SO_4$] (+) | ECM/[Na] (+) |
| --- | Ā/[Mg] (-) | ECM/[nssS] (+) | ECM/[$SO_4$] (+) | Ā/[nssS] (-) | ECM/[nssS] (+) | Ā/ECM (+) |
| --- | Ā/[Cl] (-) | Ā/[Ce] (-) | Ā/[Mg] (-) | Ā/[Ce] (-) | Ā/[Mg] (-) | Ā/[nssCa] (+) |
| ***KEY*** | ECM/[$SO_4$] (+) | Ā/[nssCa] (-) | Ā/[Na] (-) | Ā/[nssCa] (-) | Ā/[$SO_4$] (-) | Ā/[nssS] (+) |
| ***SSS Rating*** | ECM/[nssS] (+) | Ā/ECM (+) | Ā/[Cl] (-) | Ā/[BC] (-) | Ā/[nssS] (-) | ECM/[Ce] (+) |
| | Ā/[SO4] (-) | Ā/[BC] (-) | ECM/[Mg] (-) | ECM/[BC] (+) | Ā/[Cl] (-) | ECM/[BC] (+) |
| **High-** | Ā/ECM (+) | ECM/[Ce] (-) | ECM/[Cl] (-) | ECM/[nssCa] (+) | Ā/[Na] (-) | ECM/[nssCa] (-) |
| **Moderate-** | Ā/[nssS] (-) | ECM/[Na] (+) | ECM/[Na] (-) | Ā/[Na] (-) | ECM/[Mg] (-) | Ā/[BC] (+) |
| **Low-** | ECM/[Na] (-) | ECM/[BC] (+) | Ā/ECM (-) | ECM/[Ce] (-) | Ā/[$NO_3$] (+) | Ā/[Ce] (+) |
| **Very Low-** | Ā/[$NO_3$] (+) | ECM/[nssCa] (-) | Ā/[$SO_4$] (-) | Ā/ECM (+) | ECM/[Na] (-) | Ā/[Na] (+) |
| --- | ECM/[Cl] (-) | --- | Ā/[nss$SO_4$] (+) | --- | Ā/ECM (-) | --- |
| --- | ECM/[Mg] (-) | --- | Ā/[$NO_3$] (-) | --- | ECM/[Cl] (-) | --- |

# Chapter 4

# Discussion

## I) Analytical Structure

Expanding upon the SSS rating scheme used to create Table 3-1, a "net scaled statistical significance" (net SSS) rating was determined for each data pair to characterize the overall correlation of data pairs across the 7 analytic frames as determined by the pairs' mean SSS rating in each analytical frame (Table 3-1). The sign of the most significant, non-zero trends for each data pair in each analytical were used to create a polarity-ratio for each data pair where the more dominant polarity of the ratio communicates the polarity of overall relationship between each data pair. Results of this assessment are tabulated in Table 4-1. These net SSS ratings form the basis for the following discussion.

**Table 4-1: Data Pair Net Scaled Statistical Significance Ratings and Sign-Ratios**

| Data Pair | Net SSS Rating | Polarity-Ratio ( + ):( - ) | Data Pair | Net SSS Rating | Polarity-Ratio ( + ):( - ) |
|---|---|---|---|---|---|
| EMC/[nssS] | High | 5 : 1 | Ā/ECM | Moderate | 4 : 2 |
| EMC/[NO3] | High | 3 : 0 | Ā/[Na] | Moderate | 1 : 6 |
| ECM/[SO4] | High | 3 : 0 | Ā/[nssS] | Moderate | 1 : 6 |
| Ā/[Mg] | High | 0 : 3 | Ā/[Cl] | Moderate | 0 : 3 |
| Ā/[nssCa] | High | 1 : 2 | Ā/[Ce] | Moderate | 1 : 2 |
| ECM/[Na] | Low | 4 : 2 | Ā/[BC] | Moderate | 1 : 2 |
| ECM/[Mg] | Low | 0 : 3 | ECM/[Cl] | Moderate | 0 : 3 |
| ECM/[Ce] | Low | 1 : 2 | ECM/[nssCa] | Moderate | 1 : 2 |
| Ā/[SO4] | Low | 0 : 3 | ECM/[BC] | Moderate | 3 : 0 |
| Ā/[NO3] | Very Low | 3 : 0 | --- | --- | --- |

**II) High Significance Trends**

The data pairs deemed highly significant in Table 4-1 include three correlations with ECM (nssS, $SO_4$, and $NO_3$) and two correlations with Ā (Mg and nssCa). The impurity species associated with conductivity data all represent acid conjugates (specifically $H_2SO_4$ and $HNO_3$) that are sourced from sea salt and aerosols. The dominantly positive relationships between conductivity and these species support the findings of several studies that characterize a strong direct relationship between acid concentration and conductivity in glacier ice (Alley et al. 1986a, Sugiyama et al. 2000, and Barnes & Wolff 2004).

The negative relationships of Ā/[nssCa] are interpreted as a proxy for dust loading and its effect on grain-area. Non-sea-salt calcium also has a low mean concentration (2.38±3.94 PPB mean value), and therefore may not have a direct physical control on grain-size. Because these data are distinguished as non-sea-salt, [nssCa] is interpreted as an impurity from a terrestrial source. As discussed by Alley et al. (1986a) and examined by Durand et al. (2006), terrestrial dust may have a significant inverse relationship with grain-area. If [nssCa] is considered a proxy for terrestrial dust, then the high significance negative relationships for Ā/[nssCa] serve as an indicator of an inverse relationship between dust concentrations and grain-size (Alley et al. 1986a and references therein).

The exclusively negative relationships of Ā/[Mg] are interpreted here as a proxy for terrestrial dust loading and its effect on grain-area. Magnesium has a low mean concentration (3.47±2.00 PPB), and therefore may not have a direct physical control on grain-size, as a more abundant impurity would. Instead, [Mg] serve as a proxy for a more prominent impurity such as terrestrial dust. A strong cross-correlation between [Mg], [nssCa], and [Ce] might better characterize magnesium as a proxy for terrestrial dust loading. While sea salt does contain some magnesium, the inverse ECM/[Mg] relationship (discussed in greater detail in Chapter 4, Part IV)

is reminiscent of the relationships of [nssCa] with grain-area and conductivity. Therefore, Mg is considered to be primarily sourced from terrestrial dust. Cross-correlation between [Mg] and dust concentration might better characterize this component of the [Mg] record.

**III) Moderate Significance Trends**

Moderately significant data pairs in Table 4-1 include several correlations with Ā (Na, Cl, nssS, Ce, and BC), three correlations with ECM (BC, nssCa, and Cl), and the correlation between Ā/ECM (Table 4-1). The negative trends of Ā/[Na] and Ā/[Cl] are interpreted to represent the effect of sea salt loading on grain-size, while the inverse relationship of Ā/[nssS] is interpreted as an indicator of aerosol loading and its effect on grain-size. These three relationships are consistent with the inverse relationship between soluble impurities and grain-area as discussed by Alley et al. (1986a,b) and Alley & Woods (1996). Correlations of Ā/[Ce] produce dominantly inverse trends. If cerium is considered a proxy for terrestrial dust loading, this relationship supports the inverse relationship between dust concentrations and grain-size as discussed by Alley et al. (1986a and references therein). The correlations between Ā/[BC] produce both direct and inverse trends, the more abundant of which are negative. While black carbon has a very low mean concentration (0.1449±0.1225 PPB) in the WDC 06A core, and therefore likely does not have direct physical control on grain-area, it does serve as a proxy for ammonium concentration (Alley pers-comm). High ammonium concentrations are characterized in other studies as inversely related to grain-area, but not strongly related for low low concentrations (Alley & Woods 1996).

Correlations involving ECM with moderate significance included ECM/[BC], ECM/[nssCa], and ECM/[Cl]. The direct relationship between conductivity and [BC] is interpreted as a proxy for a direct relationship between ammonium ($NH_4$) and conductivity, if [BC] is indeed a proxy for only [$NH_4$]. This interpretation follows the same rationale as discussed for the relationship of Ā/[BC]. If [nssCa] is considered a proxy for terrestrial dust, then the inverse relationship of EMC/[nssCa] supports the observations of Taylor et al. (1993), where dust increases ice alkalinity and reduces conductivity. The inverse correlations of ECM/[Cl] are weakly supported in all analytical frames. While the model sets for this relationship have some statistical significance (having moderate sample fractions in the VTS and VTS100 frames), the polarity sums of these model sets are all -1, meaning a high degree of variability in the polarities of the model sets. As such, the relationship of ECM/[Cl] determined in this work was interpreted as a poor correlation.

Correlations of Ā/ECM had both positive and negative trends, the more abundant and statistically significant of which were positive. The mixture of trend polarities indicates that this is a noisy relationship dictated by both impurity loading and impurity speciation. As suggested by the relationships characterized in this work and in other studies, grain-area is likely reduced by increased impurity loading, while electrical conductivity is likely reduced by alkaline impurities and increased acidic impurities (Alley et al. 1986a, Alley & Woods 1996, Taylor et al. 1993, and Sugiyama et al. 2000). The noisy positive trend that characterizes the relationship of Ā/ECM in this work may suggest that terrestrial dust has a more prominent influence on grain area than previously thought. Additional research is needed to better characterize this hypothesized relationship.

**IV) Low and Very Low Significance Trends**

Data pairings with low statistical significance in Table 4-1 include three correlations with ECM (Ce, Mg, and Na) and one correlation with grain-area ($SO_4$). If the observed negative trends for ECM/[Ce] are noisy but real, and cerium is considered a proxy for terrestrial dust, then the relationship of [Ce] and ECM observed in this work corroborates the conductivity reduction caused by alkaline dust as discussed by Taylor et al. (1993). The inverse relationships characterized by ECM/[Mg] may represent another, although noisy, proxy for terrestrial dust. As previously discussed Mg is partially sourced from terrestrial dust, which has an inverse relationship with conductivity (Taylor et al. 1993). This theory is further supported by the relationships between ECM/[Cl] and ECM/[Na]. Both sodium and chloride are dominantly soured from sea salt, and both are characterized as having weak correlations with ECM. This system of relationships indicates that sea-salt does not have as large a control conductivity as acids and alkaline dust, thus suggesting that the relationship between magnesium and conductivity is one based upon the terrestrial dust component of [Mg] in the WDC 06A core.

Similarly, models of Ā/[SO4] produce negative trends, but their low statistical significance suggests a large amount of variability when depth correlating these data. This might still fall within the “noisy” part of the description from Alley and Woods’ (1996) “noisy yet significant” inverse correlation between impurity concentrations and Ā. The relationships between these data might be improved through higher resolution impurity data in order to capture finer scale spatial variations within a vertical thin section. The correlation of Ā/[$NO_3$] produces positive trends with very low statistical value. This suggests little or no correlation value at all reference frames between these two datasets while using the methods employed in this work.

**V) Summary**

The relationships between grain-area, impurity loading, and electrical conductivity characterized in this work for the WDC 06A ice core support the interpretations of several independent studies on ice cores from Greenland and Antarctica (including Alley et al. 1986a,b, Taylor et al. 1993, Alley & Woods 1996, Sugiyama et al. 2000, Barnes & Wolff 2004, and Durand et al. 2006). Soluble impurities associated with sea salt and aerosols, specifically Na, Cl, $SO_4$, nssS, show significant inverse relationships with grain-area. Black carbon also shows a noisy, inverse relationship with grain-area as well. Soluble impurities associated with acids, specifically nssS, $NO_3$, and $SO_4$ show significant direct relationships with conductivity. Impurities interpreted as proxies for terrestrial dust, specifically nssCa and Ce, but also Mg (to an extent), show significant inverse relationships to both grain-size and conductivity. Impurity species associated with sea salt (Na, Cl, and possibly some Mg) show weak correlation to conductivity, suggesting that sea salt has a less significant control over conductivity than acidic salts, acidic aerosols, and alkaline dust. Grain-area and ECM are characterized as having a noisy, direct relationship that likely reflects the interplay of conductivity enhancing and reducing impurities, both of which reduce grain-area as characterized above. The overall positive trend of Ā/ECM may suggest that terrestrial dust has more influence on conductivity than acids when examining large sections of the WDC 06A core, but this would require additional investigation to determine with any certainty.

## VI) Suggestions for Future Research

This work serves as a starting point for several lines of additional investigation into both strong and weak relationships characterized here. Datasets from strong correlations should be the subject of additional statistical analyses such that these relationships might be better characterized, quantified, and compared closely with similar relations from other ice cores. These analyses and comparisons might serve to strengthen past observations, provide new insights, or possibly identify unique features of the WDC 06A core not previously observed in other cores. Such analysis might include, but is not limited to, an empirical orthogonal function (EOF) analysis to determine primary and secondary signals communal to these data (Alley pers-comm). Chemical species associated with the major impurity sources for glacier ice (sea salt, terrestrial dust, and aerosols) should be cross-correlated to better constrain the relative contribution of these sources to the observed impurity concentrations. Additionally, specific attention should also be paid to the Ā/ECM system as it has possible implications for determining the relative contributions of different impurity species to both grain growth and conductivity trends.

When grain-area, impurity concentration, and ECM records become available for sections of the WDC 06A core deeper than 2683m, these data should be assessed in a similar manner to expand upon the spatial scope of this work. Similarly, should higher resolution impurity concentration records become available they might serve to increase data resampling spatial resolution, which could improve the characterization of relationships addressed in this work. Moreover, these data should be addressed with statistical methods which expand those employed here, using this work as a guide to tailor analytic methods to specific relationships.

# Chapter 5

# Conclusion

The statistical analyses conducted in this work, while dominantly qualitative, characterized several significant relationships between grain-area, impurity, and ECM data for the WAIS Divide 06A ice core, Antarctica, that corroborate the results of similar analyses on ice cores in central Greenland, particularly GISP2, and Antarctica. Impurities sourced from sea salts, aerosols (with the exception of $NO_3$), and terrestrial dust show significant inverse relationships with grain-area, thus supporting the studies of Alley et al. (1986a,b), Alley & Woods (1996), and Durand et al. (2006). Correlations between acidic impurities (nssS, $NO_3$, and $SO_4$) and ECM are characterized here as significant direct relationships, which supports the findings of several studies (including Sugiyama et al. 2000, and Barnes & Wolff 2004). Proxies for terrestrial dust (nssCa, Ce, and some Mg) are characterized as having significant inverse relationships with conductivity, which supports the findings of Taylor et al. (1993). Grain-area and ECM are characterized as a noisy relationship that may be indicative of impurity loading and speciation, which requires additional investigation or the corroboration of other studies. In general, the data from WAIS Divide indicate that acidic impurities increase ECM, dust decreases ECM, and that almost all impurities decrease grain-growth rates.

Many of the relationships characterized in this work act the starting point for lines of additional research, particularly the relationships between impurities associated with each impurity source (sea salt, terrestrial dust, and aerosols), and the relationship between grain-area and conductivity (Ā/ECM). Significant relationships characterized in this work should be quantified using additional statistical analyses, which would allow more descriptive comparisons between the observations of this work and those described by other studies on glacier ice in Greenland and Antarctica.

The characterizations made in this work, related studies, and similar independent studies on glacier ice help to constrain the effect of impurity loading on grain-area. By better understanding the degree of influence impurity loading has on normal grain-growth, this parameter can be accounted for when interpreting the degree and manner of deformation on which flow-laws are based. By constraining these relationships we are able to better model ice sheets, thereby improving our understanding and models of past, present, and future atmospheric and cryospheric dynamics.

# Chapter 6

# Appendices

## Appendix A: Tables

**Table 6-1: Shallow Linear Regression Statistics: S-MVTS Analytical Frame**

| | Statistics | | Parameter 1 | | Parameter 2 | |
|---|---|---|---|---|---|---|
| **Data Pairing** | **Slope** | **P-Value** | **Mean** | **St. Dev** | **Mean** | **St. Dev** |
| Ā/[Na] | -496.0261 | 0.0006 | 0.0714 $cm^2$ | 0.0102 $cm^2$ | 19.3821 PPB | 19.5004 PPB |
| Ā/[Mg] | -58.3951 | 0.0024 | 0.0714 $cm^2$ | 0.0102 $cm^2$ | 3.4653 PPB | 1.9987 PPB |
| Ā/[$SO_4$] | -243.3744 | 0.1124 | 0.0714 $cm^2$ | 0.0102 $cm^2$ | 27.1456 PPB | 13.2846 PPB |
| Ā/[Cl] | -683.5787 | 0.0040 | 0.0714 $cm^2$ | 0.0102 $cm^2$ | 34.1210 PPB | 34.2262 PPB |
| Ā/[nss$SO_4$] | -133.3169 | 0.4526 | 0.0714 $cm^2$ | 0.0102 $cm^2$ | 22.2696 PPB | 14.1700 PPB |
| Ā/[$NO_3$] | -41.8623 | 0.7419 | 0.0714 $cm^2$ | 0.0102 $cm^2$ | 29.7143 PPB | 9.9564 PPB |
| Ā/ECM | 3.5534 | 0.3109 | 0.0714 $cm^2$ | 0.0102 $cm^2$ | 48.756 µS | 11.534 µS |
| ECM/[nss$SO_4$] | 3.2336 | 0.0372 | 48.756 µS | 11.534 µS | 22.2696 PPB | 14.1700 PPB |
| ECM/[$NO_3$] | 5.1677 | 0.0000 | 48.756 µS | 11.534 µS | 29.7143 PPB | 9.9564 PPB |
| ECM/[$SO_4$] | 3.5971 | 0.0042 | 48.756 µS | 11.534 µS | 27.1456 PPB | 13.2846 PPB |
| ECM/[Na] | -1.0240 | 0.4636 | 48.756 µS | 11.534 µS | 19.3821 PPB | 19.5004 PPB |
| ECM/[Mg] | -0.0144 | 0.9374 | 48.756 µS | 11.534 µS | 3.4653 PPB | 1.9987 PPB |
| ECM/[Cl] | -0.5094 | 0.8452 | 48.756 µS | 11.534 µS | 34.1210 PPB | 34.2262 PPB |

**Table 6-2: Deep Linear Regression Statistics: D-MVTS Analytical Frame**

| | Statistics | | Parameter 1 | | Parameter 2 | |
|---|---|---|---|---|---|---|
| **Data Pairing** | **Slope** | **P-Value** | **Mean** | **St. Dev** | **Mean** | **St. Dev** |
| Ā/[nssS] | -122.71326 | 0.00331 | 0.0628 $cm^2$ | 0.0134 $cm^2$ | 18.3010 PPB | 10.6384 PPB |
| Ā/[Na] | -814.45008 | 0.00000 | 0.0628 $cm^2$ | 0.0134 $cm^2$ | 29.3087 PPB | 21.0759 PPB |
| Ā/[nssCa] | -190.33728 | 0.00000 | 0.0628 $cm^2$ | 0.0134 $cm^2$ | 2.3781 PPB | 3.9416 PPB |
| Ā/[BC] | -1.13204 | 0.29581 | 0.0628 $cm^2$ | 0.0134 $cm^2$ | 0.1449 PPB | 0.1225 PPB |
| Ā/[Ce] | -0.17316 | 0.00001 | 0.0628 $cm^2$ | 0.0134 $cm^2$ | 0.0027 PPB | 0.0046 PPB |
| Ā/ECM | 2.13089 | 0.28635 | 0.0628 $cm^2$ | 0.0134 $cm^2$ | 11.675 µS | 6.911 µS |
| ECM/[nssS] | 6.31035 | 0.00901 | 11.675 µS | 6.911 µS | 18.3010 PPB | 10.6384 PPB |
| ECM/[Na] | 3.40716 | 0.59437 | 11.675 µS | 6.911 µS | 29.3087 PPB | 21.0759 PPB |
| ECM/[nssCa] | -0.26607 | 0.61507 | 11.675 µS | 6.911 µS | 2.3782 PPB | 3.9417 PPB |
| ECM/[Ce] | -0.00039 | 0.50620 | 11.675 µS | 6.911 µS | 0.0026637 PPB | 0.00463485 PPB |
| ECM/[BC] | 0.01994 | 0.59813 | 11.675 µS | 6.911 µS | 0.1449 PPB | 0.1225 PPB |

### Table 6-3: Shallow Linear Regression Statistics: S-VTS100 Analytical Frame

| P-Value Filter | No Filter | | | | P-Value ≤ 0.3 | | | | P-Value ≤ 0.1 | | | |
|---|---|---|---|---|---|---|---|---|---|---|---|---|
| **Data Pairing** | **(+)** | **(-)** | **Polarity Sum** | **SF** | **(+)** | **(-)** | **Polarity Sum** | **SR** | **(+)** | **(-)** | **Polarity Sum** | **SR** |
| Ā/[Na] | 3 | 4 | -1 | 1 | 1 | 2 | -1 | 0.43 | 0 | 1 | -1 | 0.14 |
| Ā/[Mg] | 3 | 4 | -1 | 1 | 1 | 2 | -1 | 0.43 | 0 | 2 | -2 | 0.29 |
| Ā/[$SO_4$] | 2 | 5 | -3 | 1 | 0 | 0 | 0 | 0.00 | 0 | 0 | 0 | 0.00 |
| Ā/[Cl] | 3 | 4 | -1 | 1 | 2 | 2 | 0 | 0.57 | 0 | 1 | -1 | 0.14 |
| Ā/[nss$SO_4$] | 4 | 3 | 1 | 1 | 0 | 0 | 0 | 0.00 | 0 | 0 | 0 | 0.00 |
| Ā/[$NO_3$] | 4 | 3 | 1 | 1 | 0 | 0 | 0 | 0.00 | 0 | 0 | 0 | 0.00 |
| Ā/ECM | 2 | 5 | -3 | 1 | 0 | 1 | -1 | 0.14 | 0 | 0 | 0 | 0.00 |
| ECM/[nss$SO_4$] | 7 | 0 | 7 | 1 | 4 | 0 | 4 | 0.57 | 3 | 0 | 3 | 0.43 |
| ECM/[$NO_3$] | 7 | 0 | 7 | 1 | 5 | 0 | 5 | 0.71 | 4 | 0 | 4 | 0.57 |
| ECM/[$SO_4$] | 7 | 0 | 7 | 1 | 4 | 0 | 4 | 0.57 | 2 | 0 | 2 | 0.29 |
| ECM/[Na] | 4 | 3 | 1 | 1 | 1 | 2 | -1 | 0.43 | 1 | 1 | 0 | 0.29 |
| ECM/[Mg] | 1 | 6 | -5 | 1 | 1 | 2 | -1 | 0.43 | 0 | 1 | -1 | 0.14 |
| ECM/[Cl] | 5 | 2 | 3 | 1 | 1 | 2 | -1 | 0.43 | 0 | 1 | -1 | 0.14 |

### Table 6-4: Deep Linear Regression Statistics: D-VTS100 Analytical Frame

| P-Value Filter | No Filter | | | | P-Value ≤ 0.3 | | | | P-Value ≤ 0.1 | | | |
|---|---|---|---|---|---|---|---|---|---|---|---|---|
| **Data Pairing** | **(+)** | **(-)** | **Polarity Sum** | **SR** | **(+)** | **(-)** | **Polarity Sum** | **SR** | **(+)** | **(-)** | **Polarity Sum** | **SR** |
| Ā/[nssS] | 4 | 10 | -6 | 1 | 1 | 7 | -6 | 0.57 | 0 | 2 | -2 | 0.14 |
| Ā/[Na] | 4 | 10 | -6 | 1 | 1 | 4 | -3 | 0.36 | 0 | 0 | 0 | 0 |
| Ā/[nssCa] | 2 | 12 | -10 | 1 | 1 | 3 | -2 | 0.29 | 0 | 2 | -2 | 0.14 |
| Ā/[BC] | 5 | 9 | -4 | 1 | 1 | 5 | -4 | 0.43 | 0 | 1 | -1 | 0.07 |
| Ā/[Ce] | 2 | 12 | -10 | 1 | 1 | 9 | -8 | 0.71 | 0 | 6 | -6 | 0.43 |
| Ā/ECM | 5 | 9 | -4 | 1 | 4 | 3 | 1 | 0.5 | 1 | 1 | 0 | 0.14 |
| ECM/[nssS] | 11 | 3 | 8 | 1 | 6 | 1 | 5 | 0.5 | 4 | 0 | 4 | 0.29 |
| ECM/[Na] | 9 | 5 | 4 | 1 | 5 | 2 | 3 | 0.5 | 4 | 0 | 4 | 0.29 |
| ECM/[nssCa] | 8 | 6 | 2 | 1 | 4 | 2 | 2 | 0.43 | 1 | 1 | 0 | 0.14 |
| ECM/[Ce] | 6 | 8 | -2 | 1 | 2 | 4 | -2 | 0.43 | 2 | 3 | -1 | 0.36 |
| ECM/[BC] | 9 | 5 | 4 | 1 | 3 | 2 | 1 | 0.36 | 1 | 0 | 1 | 0.07 |

### Table 6-5: Shallow Linear Regression Statistics: S-VTS Analytical Frame

| P-Value Filter | No Filter | | | | P-Value≤0.3 | | | | P-Value ≤ 0.1 | | | |
|---|---|---|---|---|---|---|---|---|---|---|---|---|
| Data Pairing | (+) | (-) | Polarity Sum | SF | (+) | (-) | Polarity Sum | SR | (+) | (-) | Polarity Sum | SR |
| Ā/[Na] | 14 | 11 | 3 | 1 | 7 | 4 | 3 | 0.44 | 1 | 2 | -1 | 0.12 |
| Ā/[Mg] | 11 | 14 | -3 | 1 | 5 | 5 | 0 | 0.4 | 0 | 3 | -3 | 0.12 |
| Ā/[$SO_4$] | 14 | 11 | 3 | 1 | 5 | 4 | 1 | 0.36 | 0 | 3 | -3 | 0.12 |
| Ā/[Cl] | 13 | 12 | 1 | 1 | 5 | 5 | 0 | 0.4 | 2 | 3 | -1 | 0.2 |
| Ā/[nss$SO_4$] | 15 | 10 | 5 | 1 | 3 | 4 | -1 | 0.28 | 1 | 1 | 0 | 0.08 |
| Ā/[$NO_3$] | 11 | 14 | -3 | 1 | 2 | 3 | -1 | 0.2 | 2 | 0 | 2 | 0.08 |
| Ā/ECM | 12 | 13 | -1 | 1 | 5 | 5 | 0 | 0.4 | 1 | 1 | 0 | 0.08 |
| ECM/[nss$SO_4$] | 17 | 8 | 9 | 1 | 6 | 1 | 5 | 0.28 | 2 | 0 | 2 | 0.08 |
| ECM/[$NO_3$] | 18 | 7 | 11 | 1 | 9 | 0 | 9 | 0.36 | 3 | 0 | 3 | 0.12 |
| ECM/[$SO_4$] | 17 | 8 | 9 | 1 | 6 | 2 | 4 | 0.32 | 2 | 0 | 2 | 0.08 |
| ECM/[Na] | 11 | 14 | -3 | 1 | 2 | 3 | -1 | 0.2 | 0 | 1 | -1 | 0.04 |
| ECM/[Mg] | 11 | 14 | -3 | 1 | 2 | 7 | -5 | 0.36 | 2 | 3 | -1 | 0.2 |
| ECM/[Cl] | 13 | 12 | 1 | 1 | 2 | 3 | -1 | 0.2 | 0 | 1 | -1 | 0.04 |

### Table 6-6: Deep Linear Regression Statistics: D-VTS Analytical Frame

| P-Value Filter | No Filter | | | | P-Value ≤ 0.3 | | | | P-Value ≤ 0.1 | | | |
|---|---|---|---|---|---|---|---|---|---|---|---|---|
| Data Pairing | (+) | (-) | Polarity Sum | SF | (+) | (-) | Polarity Sum | SR | (+) | (-) | Polarity Sum | SR |
| Ā/[nssS] | 31 | 30 | 1 | 1.00 | 6 | 8 | -2 | 0.23 | 3 | 1 | 2 | 0.07 |
| Ā/[Na] | 32 | 29 | 3 | 1.00 | 7 | 7 | 0 | 0.23 | 3 | 3 | 0 | 0.10 |
| Ā/[nssCa] | 28 | 32 | -4 | 1.00 | 9 | 7 | 2 | 0.27 | 7 | 3 | 4 | 0.17 |
| Ā/[BC] | 25 | 36 | -11 | 1.00 | 11 | 13 | -2 | 0.39 | 4 | 3 | 1 | 0.11 |
| Ā/[Ce] | 31 | 30 | 1 | 1.00 | 13 | 11 | 2 | 0.39 | 5 | 4 | 1 | 0.15 |
| Ā/ECM | 26 | 33 | -7 | 1.00 | 8 | 5 | 3 | 0.22 | 4 | 0 | 4 | 0.07 |
| ECM/[nssS] | 34 | 23 | 11 | 1.00 | 13 | 8 | 5 | 0.37 | 6 | 1 | 5 | 0.12 |
| ECM/[Na] | 29 | 28 | 1 | 1.00 | 13 | 9 | 4 | 0.39 | 8 | 1 | 7 | 0.16 |
| ECM/[nssCa] | 28 | 28 | 0 | 1.00 | 12 | 11 | 1 | 0.41 | 4 | 5 | -1 | 0.16 |
| ECM/[Ce] | 31 | 26 | 5 | 1.00 | 16 | 8 | 8 | 0.42 | 10 | 2 | 8 | 0.21 |
| ECM/[BC] | 32 | 25 | 7 | 1.00 | 12 | 13 | -1 | 0.44 | 6 | 3 | 3 | 0.16 |

### Table 6-7: Vertical Thin Section Sample Log

| From Alley & Fitzpatrick 2012, NICL 2012, Fitzpatrick pers-comm | | | | | | |
|---|---|---|---|---|---|---|
| VTS ID # | Top Depth (m) | Bottom Depth (m)2 | Depth Range (cm) | Grain Count | No. Resampled Data Points | 100m VTS Bin # |
| 580 | 579.004 | 579.1 | 9.60127 | 914 | 5 | 1 |
| 605 | 603.5572 | 603.6458 | 8.86177 | 789 | 4 | 1 |
| 625 | 623.3179 | 623.3948 | 7.6902 | 839 | 4 | 1 |
| 665 | 662.8721 | 662.958 | 8.58347 | 803 | 4 | 1 |
| 685 | 682.943 | 683.0299 | 8.6906 | 905 | 4 | 2 |
| 705 | 702.0031 | 702.0873 | 8.4272 | 919 | 3 | 2 |
| 725 | 722.0001 | 722.0847 | 8.46914 | 718 | 4 | 2 |
| 765 | 762.0272 | 762.1153 | 8.8135 | 857 | 4 | 2 |
| 786 | 783.015 | 783.1017 | 8.67287 | 830 | 3 | 3 |
| 825 | 822.3076 | 822.393 | 8.53535 | 829 | 3 | 3 |
| 865 | 863.0218 | 863.1032 | 8.13372 | 812 | 3 | 3 |
| 885 | 883.03 | 883.1193 | 8.9318 | 771 | 4 | 4 |
| 945 | 943.0598 | 943.1535 | 9.37073 | 1026 | 3 | 4 |
| 965 | 962.5794 | 962.6645 | 8.50599 | 840 | 4 | 4 |
| 985 | 982.522 | 982.6068 | 8.47937 | 725 | 4 | 5 |
| 1005 | 1003.535 | 1003.626 | 9.09513 | 776 | 3 | 5 |
| 1045 | 1042.523 | 1042.618 | 9.45549 | 839 | 4 | 5 |
| 1064 | 1062.108 | 1062.197 | 8.84032 | 1144 | 3 | 5 |
| 1085 | 1082.345 | 1082.43 | 8.52661 | 1085 | 3 | 6 |
| 1104 | 1102.004 | 1102.092 | 8.85243 | 1241 | 3 | 6 |
| 1125 | 1123.512 | 1123.6 | 8.7467 | 885 | 4 | 6 |
| 1185 | 1184.1 | 1184.186 | 8.64724 | 1087 | 4 | 7 |
| 1204 | 1203.202 | 1203.29 | 8.8013 | 1248 | 3 | 7 |
| 1224 | 1224.003 | 1224.093 | 9.06319 | 1146 | 4 | 7 |
| 1245 | 1244.803 | 1244.892 | 8.96213 | 1166 | 3 | 7 |
| 1360 | 1362.416 | 1362.505 | 8.88082 | 519 | 4 | 8 |
| 1380 | 1382.764 | 1382.86 | 9.64152 | 798 | 5 | 8 |
| 1400 | 1402.772 | 1402.867 | 9.56845 | 638 | 4 | 9 |
| 1420 | 1422.278 | 1422.338 | 5.99017 | 950 | 3 | 9 |
| 1440 | 1442.746 | 1442.842 | 9.59482 | 660 | 5 | 9 |
| 1460 | 1462.765 | 1462.86 | 9.48943 | 707 | 5 | 9 |
| 1480 | 1482.744 | 1482.838 | 9.44183 | 767 | 5 | 9 |

| 1500 | 1502.714 | 1502.811 | 9.66744 | 737 | 5 | 10 |
|---|---|---|---|---|---|---|
| 1520 | 1522.661 | 1522.76 | 9.84366 | 760 | 5 | 10 |
| 1540 | 1542.791 | 1542.884 | 9.33275 | 516 | 4 | 10 |
| 1560 | 1562.815 | 1562.911 | 9.57895 | 702 | 5 | 10 |
| 1580 | 1582.821 | 1582.912 | 9.07448 | 534 | 5 | 10 |
| 1600 | 1602.844 | 1602.937 | 9.26186 | 653 | 5 | 11 |
| 1620 | 1621.874 | 1621.968 | 9.42873 | 676 | 4 | 11 |
| 1640 | 1642.889 | 1642.985 | 9.57271 | 506 | 5 | 11 |
| 1660 | 1662.911 | 1663.006 | 9.52261 | 579 | 4 | 11 |
| 1680 | 1682.923 | 1683.017 | 9.3712 | 508 | 5 | 11 |
| 1700 | 1702.944 | 1703.04 | 9.58288 | 482 | 5 | 12 |
| 1720 | 1722.959 | 1723.056 | 9.71763 | 562 | 5 | 12 |
| 1740 | 1742.974 | 1743.069 | 9.52491 | 684 | 4 | 12 |
| 1760 | 1762.984 | 1763.079 | 9.45435 | 549 | 5 | 12 |
| 1780 | 1783.009 | 1783.105 | 9.60816 | 670 | 5 | 12 |
| 1800 | 1803.004 | 1803.1 | 9.56858 | 600 | 5 | 13 |
| 1820 | 1823.024 | 1823.117 | 9.32367 | 575 | 5 | 13 |
| 1860 | 1863.088 | 1863.18 | 9.21434 | 598 | 5 | 13 |
| 1880 | 1883.12 | 1883.211 | 9.13892 | 567 | 5 | 13 |
| 1900 | 1903.137 | 1903.234 | 9.70502 | 678 | 5 | 14 |
| 1920 | 1923.182 | 1923.277 | 9.48327 | 573 | 5 | 14 |
| 1940 | 1943.096 | 1943.19 | 9.4027 | 625 | 5 | 14 |
| 1980 | 1983.253 | 1983.347 | 9.45926 | 567 | 4 | 14 |
| 2000 | 2003.25 | 2003.343 | 9.28628 | 457 | 4 | 15 |
| 2020 | 2023.264 | 2023.363 | 9.84501 | 639 | 5 | 15 |
| 2040 | 2043.264 | 2043.358 | 9.41315 | 578 | 5 | 15 |
| 2080 | 2083.255 | 2083.351 | 9.58165 | 767 | 5 | 15 |
| 2100 | 2103.157 | 2103.25 | 9.33202 | 938 | 5 | 16 |
| 2120 | 2123.266 | 2123.361 | 9.44793 | 886 | 5 | 16 |
| 2140 | 2143.258 | 2143.352 | 9.37743 | 690 | 5 | 16 |
| 2160 | 2163.252 | 2163.345 | 9.21971 | 562 | 4 | 16 |
| 2180 | 2183.246 | 2183.339 | 9.28947 | 724 | 5 | 16 |
| 2200 | 2203.241 | 2203.333 | 9.21241 | 609 | 5 | 17 |
| 2220 | 2223.243 | 2223.338 | 9.48097 | 760 | 5 | 17 |
| 2240 | 2243.241 | 2243.337 | 9.60827 | 699 | 5 | 17 |
| 2260 | 2263.236 | 2263.334 | 9.79885 | 821 | 5 | 17 |

| | | | | | | |
|---|---|---|---|---|---|---|
| 2280 | 2283.25 | 2283.342 | 9.20998 | 741 | 5 | 17 |
| 2300 | 2303.224 | 2303.319 | 9.53313 | 799 | 5 | 18 |
| 2320 | 2323.228 | 2323.324 | 9.54897 | 818 | 5 | 18 |
| 2340 | 2343.241 | 2343.334 | 9.22914 | 817 | 5 | 18 |
| 2360 | 2363.227 | 2363.324 | 9.72401 | 876 | 5 | 18 |
| 2380 | 2383.241 | 2383.338 | 9.62099 | 917 | 5 | 18 |
| 2400 | 2403.25 | 2403.343 | 9.29573 | 743 | 4 | 19 |
| 2420 | 2423.269 | 2423.365 | 9.63235 | 1311 | 5 | 19 |
| 2440 | 2443.261 | 2443.355 | 9.45451 | 1403 | 5 | 19 |
| 2460 | 2463.274 | 2463.371 | 9.72771 | 1669 | 5 | 19 |
| 2480 | 2484.17 | 2484.266 | 9.5316 | 1015 | 4 | 19 |
| 2500 | 2503.316 | 2503.412 | 9.57274 | 1666 | 5 | 20 |
| 2520 | 2523.277 | 2523.375 | 9.75136 | 1607 | 5 | 20 |
| 2540 | 2543.291 | 2543.386 | 9.50279 | 1434 | 4 | 20 |
| 2560 | 2563.302 | 2563.399 | 9.70392 | 1660 | 5 | 20 |
| 2605 | 2603.314 | 2603.412 | 9.82412 | 1998 | 5 | 21 |
| 2625 | 2623.323 | 2623.411 | 8.80362 | 1807 | 5 | 21 |
| 2645 | 2643.335 | 2643.434 | 9.91425 | 1835 | 5 | 21 |
| 2665 | 2663.346 | 2663.445 | 9.87958 | 1998 | 5 | 21 |
| 2685 | 2683.371 | 2683.468 | 9.69754 | 1998 | 4 | 21 |

## WORKS CITED


Alley, R. B., J.H Perepezko and C. R. Bentley. 1986a. Grain growth in polar ice: I. Theory. *J. Glaciology*, **32**(112), 415-424.

Alley, R. B., J.H Perepezko and C. R. Bentley. 1986b. Grain growth in polar ice: II. Application. *J. Glaciology*, **32**(112), 425-433.

Alley, R. B. 1992. Flow-law hypotheses for ice-sheet modeling. *J. Glaciology*, **38**(129), 245-256.

Alley, R. B., A. J. Gow and D. A. Meese. 1995. Instruments and Methods Mapping c-axis fabrics to study physical processes in ice. *J. Glaciology*, **41**(137), 197-203.

Alley, R. B. and G. A. Woods. 1996. Impurity influence on normal grain growth in the GISP2 ice core, Greenland. *J. Glaciology*, **42**(141), 255-260.

Alley, R. B. and Fitzpatrick, J. J. 2012. WDC06A Mean Grain Sized 120-3400m. *WAIS Divide Investigators Portal*, http://waisdivide.unh.edu

Alley, R. B. 2011-2013. *Personal Communications*. E-mail and conference.

Barnes, P. R. F. and E. W. Wolff. 2004. Distribution of soluble impurities in cold glacial ice. *J. Glaciology*, **50**(170), 311-324.

Cole-Dai, J. 2012. Major ion chemistry 577m-1300m. *WAIS Divide Investigators Portal*, http://waisdivide.unh.edu

Conway, H. WDC-sitemap-maparea. *WAIS Divide Investigators Portal*, http://waisdivide.unh.edu. Digital Image. University of Washington

Cuffey, K. M. and W. S. B. Paterson. 2010. The Physics of Glaciers - 4th Ed. *Elsevier*. Burlington, MA.

Durand, G. and 10 others. 2006. Effects of impurities on grain growth in cold ice sheets. *J. Geophysical Research*, 111, F01015.

Fitzpatrick, J. J. and 4 others. 2012. Grain Area Statistics (580m-2685m). *Personal Communication*. E-mail and conference.

Fitzpatrick, J. J., 2013. Digital image processing and image analysis for glacier ice. *US Geological Survey Techniques and Methods Report (in review)*, 22 p.

Gow, A. J. 1969. On the rates of growth of grains and crystals in South Polar firn. *J. Glaciology*, **8**(53), 241-252.

McConnell, J. 2012. Select Trace and Ultra-Trace Chemistry 1300m-2700m. *Personal Communication*. E-mail.

National Ice Core Laboratory (NICL). 2012. *WDC 06A Sample Database*. http://nicl.usgs.gov

Taylor, K. C. and 9 others. Electrical Conductivity Measurements from the GISP2 and GRIP Greenland Ice Cores. *Nature* 366.6455 (1993): 549-52. PDF.

Taylor, K. 2011. WDC06A electrical measurements 0-3331 meters. *WAIS Divide Investigators Portal*, http://waisdivide.unh.edu

Taylor, K. 2013. Personal Communication. E-mail. 2/20/2013.

Sugiyama, K. and 7 others. 2000. Measurement of electrical conductance in ice cores by AC-ECM method. *Physics of Ice Core Records*. 173-184. Hokkaido University Press, Sapporo.

Woods, G. A. 1994. Grain growth behavior of the GISP2 ice core from central Greenland. University Park, PA, Pennsylvania State University. Earth System Science Center. (Technical Report 94-002.)

# ACADEMIC VITA

Nathan T. Stevens

nts5045@psu.edu

---

**Education**

B.S., Geosciences, 2013, The Pennsylvania State University, University Park, Pennsylvania

**Honors and Awards**

Dean's List, The Pennsylvania State University, Department of Geosciences, 2009-Present

Various Merit Based Scholarships, The Pennsylvania State University, 2009-Present

- Schreyer Honors College
  - Schreyer Honors College Global Ambassador Scholarship: 2011
- Department of Geosciences
  - James and Nancy Hedberg Scholarship: 2012-2013
  - Henry Reif Jr. Endowment in Geosciences: 2012
  - George Ellis Scholarship: 2011-2012
  - Ben Howell Geosciences Award: 2011
  - Joseph Berg Award – Geoscience: 2010-11
- College of Earth and Mineral Sciences
  - Bruce Miller Scholarship in the Earth and Mineral Sciences: 2012-13
  - Dean's Freshman Scholarship: 2009-2010

Eagle Scout, Cradle of Liberty Council, Montgomery County, Pennsylvania, 2007

**Association Memberships/Activities**

- American Association of Petroleum Geologists (AAPG), Penn State Student Chapter
- Geological Society of America (GSA), Student Member
- Penn State Ice and Climate Exploration Group, Research Assistant

**Professional/Research Experience**

WAIS Divide 06A Ice Core Physical Properties
*Earth & Environmental Systems Institute, University Park, PA*

- Research Assistant
  *October 2010- Present*
  - Produced bubble number density statistics in the continuation of the work of Matt Spencer (Journal of Glaciology, 2006) and the Masters and ongoing work by John Fegyveresi.
  - Produced grain boundary geometry statistics in conjunction with the work of Joan Fitzpatrick (USGS).
  - Investigated grain-bubble geometry relationship statistics in conjunction with the ongoing work of Joan Fitzpatrick (USGS).
  - Currently researching the influence of impurity loading on normal grain growth and conductivity in the WAIS Divide 06A Ice Core.
- NICL Core Processor
  *June 2011*
  - Aided in the handling and processing of the 2010-11 season cores. Duties included preparing chemistry samples for archival and producing thin-section samples for physical properties investigations.

United States Geological Survey
*USGS Exton Field Office, Exton, PA*

- Hydrologic Aid
  *June 2010 – August 2010*
  - Assisted hydrologic technicians in monitoring and maintaining the surface water monitoring network serving Philadelphia, Chester, Delaware, and Montgomery Counties.
  - Operated Acoustic Doppler Profilers, In-Situ Water Quality Sondes, and monitoring station instrumentation.

**Field Experience**

Penn State Geosciences Field Camp
*May-July 2012*

- Exercises Conducted:
  - Sequence Stratigraphy of the Book Cliffs around Helper, UT
  - Quaternary Geology of Lake Bonneville near Tooele, UT
  - Structural and Sedimentological Mapping of Elk Basin, WY
  - Mapping of the Challis Volcanic Series, Salmon-Challis National Forest, ID,
  - Sevier Thrust Structural Mapping at Alta, UT
  - Alta Stock Metamorphic Petrology and Structural Mapping, Alta, UT.

Penn State Structural Geology

*Spring 2012*

- Exercises Conducted:
  - Whipple Dam Structural Mapping, Whipple Dam State Park, PA
  - Barree Folds Structural Study, Barree, PA
  - Nittany Anticlinorium Structural Mapping, Happy Valley, PA

Penn State Earth History

*Spring 2011*

- Exercises Conducted:
  - Geologic Evolution of Eastern Pennsylvania, PA
  - Sedimentology of Central Pennsylvania, Near State College, PA

**Research Interests**

My interests lay in glaciology, particularly the interactions between the cryosphere and other Earth-Systems. In addition to this project, I am involved in several projects including paleoclimate interpretation from ice cores and quantification of grain-growth and bubble-migration patterns in the WAIS Divide 06A ice core. My upcoming projects include an investigation into crustal dynamics under continental ice sheets during ice-age cycles.

**Referenced Presentations**

West Antarctic Ice Sheet Divide Core Annual Meeting, La Jolla, CA, WAIS Divide Physical Properties Progress: Layers, Grains, Bubbles & More, R.B.Alley, J.M. Fegyveresi, J.J. Fitzpatrick, M.K. Spencer, D.E. Voigt, I. Hong,D. Laurel, A. McLarahmore and N.T. Stevens, Sep. 28, 2011.

**Publications and Papers**

Mercier, O. R., Stevens, N., & Toia, A. (2012). Mātauranga Māori and the DIKW Hierarchy: A Conversation on Interfacing Knowledge Systems. *MAI Journal*, 1(2), 103-116. http://journal.mai.ac.nz/